# Supplementary Information

# Versatile template-directed synthesis of gold nanocages with a predefined number of the windows

Céline Hubert,[a,b] Cyril Chomette,[a] Anthony Desert,[a] Alexandra Madeira,[a] Adeline Perro,[c] Ileana Florea,[d] Dris Ihaiawakrim,[d] Ovidiu Ersen,[d] Anna Lombardi,[e] Etienne Pertreux,[e] Fabien Vialla,[e] Paolo Maioli,[e] Aurélien Crut,[e] Natalia Del Fatti,[e] Fabrice Vallée,[e] Jérôme Majimel,[a] Serge Ravaine,*[b] Etienne Duguet*[a] and Mona Tréguer-Delapierre*[a]

[a]Univ. Bordeaux, CNRS, CRPP, UMR 5031, 33600 Pessac, France
[b]Univ. Bordeaux, CNRS, ISM, UMR 5255, 33400 Talence, France
[c]Univ. Bordeaux, CNRS, ICMCB, UMR 5026, 33600 Pessac, France
[d]IPCMS, UMR 7504 CNRS - Université de Strasbourg, 67034 Strasbourg, France
[e] FemtoNanoOptics group, Université de Lyon, CNRS, Université Claude Bernard Lyon 1, Institut Lumière Matière, F-69622 Villeurbanne, France

## 1 – Materials and methods

Note: All chemical procedures described below must be performed in a fume hood. Researchers must wear appropriate personal protective equipment (PPE) including lab coat, gloves, and safety glasses or goggles.

### Chemicals

Absolute ethanol (Sigma-Aldrich), ammonium hydroxide (28–30% in water, SDS), cyclohexane (HPLC grade, Sigma-Aldrich), formaldehyde (reagent grade, Sigma-Aldrich), gold(III) chloride trihydrate ($HAuCl_4.3H_2O$, Sigma-Aldrich, 99.9%), hydrofluoric acid (HF, Aldrich), methacryloxymethyltriethoxysilane (MMS, 97%, ABCR), N-[3-(trimethoxysilyl)propyl]ethylenediamine (EDPS, 97%, Aldrich), polyvinylpyrrolidone (PVP, average mol. wt. 29,000, Aldrich), potassium carbonate $K_2CO_3.1.5H_2O$ (Alfa Aesar, 95%), sodium dodecylsulfate (SDS, 99%, Aldrich), sodium hydroxide (Sigma-Aldrich, 98%), sodium persulfate (99%, Aldrich), stearic acid (Sigma-Aldrich, 95%), styrene (99%, Aldrich), Synperonic® NP30 (Aldrich), tetraethoxysilane (TEOS, >99%, Fluka), tetrahydrofuran (THF, Sigma-Aldrich) tetrakis(hydroxymethyl)phosphonium chloride (THPC, 80%, Aldrich) were used as received. Deionized water with a resistivity of 18.2 Ohm cm at 25 °C was obtained with a MilliQ system (Millipore).

### Precursors

#### Synthesis of the spherical silica particles

We used a two-stage protocol already described in detail in reference 1 to synthesize highly monodisperse silica particles. The first stage was the synthesis of pre-seeds. In the second stage, we regrew the silica pre-seeds to get particles of a larger diameter and a polydispersity index (PDI) of 1.002. The dry extract method allowed us to determine the silica concentration and to calculate the final concentration of the silica particles $1.47 \times 10^{-16}$ $L^{-1}$.

#### Synthesis of the spherical silica particles

We used these silica particles to prepare batches of the silica/polystyrene templates with a predetermined number of polystyrene (PS) satellite nodules according to a previously developed procedure.[1,2,3,4] This procedure consists of the emulsion polymerization of styrene performed in the presence of silica nanoparticles surface-modified with methacryloxyalkyl groups as seeds. The characteristics of the batches of multipods used, dispersed in water, are listed in Table S1 (page 5).

**Synthesis of the silica-coated iron oxide nanoparticles**

They were prepared according to a protocol initially reported by Li and coworkers,[5] adapted here to iron oxide nanoparticles obtained through the Massart's route[6] and consolidated in a silica shell after a protocol optimized by Adumeau.[7] Briefly, the iron oxide nanoparticles were stabilized with stearic acid in cyclohexane, dispersed in water in presence of SDS, emulsified under ultrasounds, and heated up to 70°C until complete evaporation of cyclohexane. The size distribution was narrowed by several cycles of centrifugation and a silica shell was grown around every magnetic nanoparticles using TEOS and ammonia as catalyst. The final batch was made of silica-coated maghemite supraparticles with an average diameter of 100 $\pm$ 20 nm including a silica shell thickness of 10 nm.

**Synthesis of the templates $SiO_2$/PS from the silica-coated iron oxide nanoparticles**

The magnetic seeds were first surface-modified with MMS at a nominal surface density of 0.5 functions per $nm^2$ in ethanol at room temperature for 3 h, then at ethanol reflux for 1 h. Because of the low amount available, the core-shell particles were mixed with MMS-modified 85-nm silica seeds in a 2.6/97.4 number ratio. It means that only 2.6 % of the prepared templates contained a magnetic core. Then the emulsion polymerization was performed at 70°C for 5 h under a nitrogen atmosphere in a thermoregulated reactor using Synperonic® NP30/SDS 95/5 at a total surfactant concentration of 3 $g.L^{-1}$, the previous seed mixture ($1.8*10^{16}$ $L^{-1}$), styrene (100 $g.L^{-1}$) and sodium persulfate (0.5 $g.L^{-1}$). The multipods were purified by dialysis against water, and then the magnetic ones were collected by using a strong permanent magnet. Their morphology was checked by transmission electron microscopy (Table S1).

**Gold nanoseeds**

We prepared them according to a procedure previously reported by Duff *et al*.[8] In a 500-mL flask, we introduced successively 227.5 mL water, 7.5 mL aqueous solution of NaOH (0.2 M) and 5 mL aqueous solution containing 60 µL THPC. The solution was homogenized during 15 min. Then, 10 mL $HAuCl_4$ (25 mM) were quickly injected in the flask under stirring. The solution turned from pale yellow to brown in few seconds indicating the formation of gold nanoparticles with an average diameter of 5 nm. After 10-min stirring, the dispersion was stored at 4°C.

**Gold plating solution**

We prepared the aqueous gold plating solution (GPS) by dissolving in water $HAuCl_4$ (0.4 g/L) and $K_2CO_3$ (1,25 g/L). Then the solution was let to age at 4°C for at least one week before use.

## 2- Electron microscopy experiments

**Transmission electron microscopy (TEM)**

Conventional transmission electron microscopy experiments were performed at the Plateforme Aquitaine de Caractérisation des Matériaux (UMS 3626, CNRS - Univ. Bordeaux) with a JEOL JEM-1400 Plus microscope operating at 80-120 kV. The samples were prepared as follows: colloidal dispersions were diluted in ethanol and one drop was deposited on a copper grid coated with a carbon membrane and let to evaporate.

**Scanning electron microscopy (SEM)**

Scanning electron microscopy (SEM) studies were carried out at the Plateforme of the laboratory ITODYS using a Zeiss SUPRA 40 microscope operated at 20 kV. Samples for SEM were prepared by deposition of particles onto a silicon substrate by drying a drop of colloidal solution in air.

**Elemental mapping by scanning transmission electron microscopy coupled to energy dispersive X-ray spectrometry (STEM-EDX)**

Chemical analysis was carried out at the Plateforme Aquitaine de Caractérisation des Matériaux by STEM coupled to EDX with a JEOL 2200 FS equipped with a field emissive gun, operating at 200 kV and with a point resolution of 0.23 nm. The samples were prepared as for conventional TEM experiments.

**Electron tomography**

Experimental data for electron tomography were acquired on a JEOL 2100F transmission electron microscope with a field emission gun operating at 200 kV. The tilt series used for computing the reconstruction was acquired in the TEM imaging

mode with a size of 1024 pixel x 1024 pixel and a pixel size of 0.25 nm. The acquisition software, plugged in the Digital Micrograph software, provides an automated acquisition of the tilt series by varying the tilt angle step-by-step and by controlling the defocusing and the specimen drift at each tilt angle. In addition, it allows a dynamical focus adjustment in order to ensure that the focus is maintained on the tilted specimen. The angular interval sampled during the acquisition was between 68 and -70°, with a tilt increment of 2°, giving a total of 70 images. Once the acquisition of the tilt series was completed, the images were aligned using a cross-correlation algorithm. The volume reconstructions were computed using simultaneous iterative reconstruction tomography (SIRT) implemented in the TomoJ software by considering 20 iterations. Visualization and quantitative analysis of the final volumes were carried out using Slicer and ImageJ software.

## 3- Characterization of optical properties

**UV-visible spectroscopy**

The absorption spectra were recorded in the range of 300–1300 nm with a UV-3600 Shimadzu UV-Vis-NIR spectrophotometer by using a 1 cm optical path quartz cells.

**Single nano-object optical spectroscopy**

The extinction cross-sections of individual nanocages were measured using spatial modulation spectroscopy (SMS).[9,10] This technique is based on the periodical displacement of a nano-object in the focal spot of a strongly focused laser beam. The resulting modulation of the transmitted light power is proportional to the extinction cross-section of the investigated nano-object, allowing the quantitative determination of the latter. Nanocage deposition on thin substrates compatible with both transmission optical and electron microscopies was achieved by spin-coating of the synthesized solutions, using parameters yielding a $<1\ \mu m^{-2}$ nano-object density (such low density being necessary for single-particle investigations, which require only one nano-object to be illuminated by the focused laser spot). Extinction measurements were performed using as light source a tunable Ti:sapphire oscillator associated with an optical parametric oscillator working in the visible and a β-barium borate (BBO) crystal performing frequency doubling, allowing light generation in the full 400-1080 nm spectral range. Linearly polarized light beams were used for nano-object illumination, their polarization direction being fixed using the combination of a quarter-wave plate and a polarizer. Beam focusing close to the diffraction limit was achieved by a microscope objective (0.75 numerical aperture, NA). Spatial modulation was performed at a frequency $f \approx 1.5$ kHz. The time-dependent transmitted light power induced by the modulation process was detected by a photodiode, its component at 2f frequency being extracted by a lock-in amplifier.

**Numerical optical simulations**

Modeling of the optical response of gold nanocages in the context of SMS experiments, i.e. deposited on a thin substrate, was performed using finite-element modeling (FEM).[11] Simulations were performed on a domain bounded by a perfectly matched layer, to avoid spurious light reflection at its borders. Nanocage geometry was defined using the average size parameters determined from electron microscopy observations, assuming regularly spaced openings. Johnson and Christy tables were used for gold dielectric function.[12] The thin substrate supporting the investigated nano-objects (40 nm thick silica or 20 nm carbon membrane) was explicitly included, and a refractive index larger than 1 (1.1 or 1.3) was used for the rest of their environment, to account for the presence of surfactants and/or residual solvent around them (similar values having been successfully used in previous studies to reproduce the extinction spectra of substrate-deposited gold nanorods and bipyramids)[13,14]. Illumination by a monochromatic linearly polarized plane wave was considered, its partial reflection on the substrate being taken into account in the definition of the illuminating field. The electromagnetic field distribution generated by nanocage illumination was numerically determined. For silica substrate (transparent), absorption and scattering cross-sections were then deduced from the computed field by integration of resistive heating over the Au-nanocage volume and of the scattered intensity through a closed surface surrounding the nanocage, respectively. The more general extinction calculation approach described in reference 14 also accounting for substrate absorption, was used in the case of carbon substrate (absorbing). Such simulations were repeated for different wavelengths and polarization directions of the incident wave, and different orientations of the nanocages relatively to their underlying substrate.

## 4- References


1 A. Perro, E. Duguet, O. Lambert, J. C. Taveau, E. Bourgeat-Lami and S. Ravaine, *Angew. Chem. Int. Ed.,* 2009, **121**, 367.
2 A. Désert, I. Chaduc, S. Fouilloux, J.C. Taveau, O. Lambert, M. Lansalot, E. Bourgeat-Lami, A. Thill, O. Spalla, S. Ravaine and E. Duguet, *Polym. Chem.* 2012, **3**, 1130.
3 A. Désert, J. Morele, J.C. Taveau, O. Lambert, M. Lansalot, E. Bourgeat-Lami, A. Thill, A.; Spalla, L. Belloni, S. Ravaine and E. Duguet, *Nanoscale*, 2016, **8**, 5454.
4 C. Hubert, C. Chomette, A. Désert, M. Sun, M. Treguer-Delapierre, S. Mornet, A. Perro, E. Duguet and S. Ravaine, *Faraday Discuss.,* 2015, **181**, 139.
5 F. Bai, D. Wang, Z. Huo, W. Chen, L. Liu, X. Liang, C. Chen, X. Wang, Q. Peng and Y. Li, *Angew. Chem. Int. Ed.,* 2007, **46**, 6650.
6 R. Massart, *IEEE Trans. Magn.* 1981, **17**, 1247.
7 L. Adumeau, *PhD Thesis, University of Bordeaux* **2015**, 113.
8 D. G. Duff, A. Baiker and P. P. Edwards, *Langmuir,* 1993, **9**, 2301A.
9 A. Arbouet, D. Christofilos, N. Del Fatti, F. Vallée, J. R. Huntzinger, L. Arnaud, P. Billaud and M. Broyer, *Phys. Rev. Lett.,* **2004**, *93*, 127401.
10 A. Crut, P. Maioli, N. Del Fatti and F. Vallée*,* **2014**, *43*, 3921.
11 A. Lombardi, M. Loumaigne, A. Crut, P. Maioli, N. Del Fatti, F. Vallée, M. Spuch-Calvar, J. Burgin, J. Majimel and M. Tréguer-Delapierre, *Langmuir,* 2012, **28**, 9027.
12 P. B. Johnson and R. W. Christy, *Phys. Rev.,* 1972, **6**, 4370.
13 Y. R. Davletshin, A. Lombardi, M. F. Cardinal, V. Juvé, A. Crut, P. Maioli, L. Liz-Marzán, F. Vallée and N. Del Fatti, *ACS Nano,* 2012, **6**, 8183.
14 E. Pertreux, A. Lombardi, I. Florea, M. Spuch-Calvar, S. Gómez-Graña, D. Ihiawakrim, C. Hirlimann, O. Ersen, J. Majimel, M. Tréguer-Delapierre, M. Hettich, P. Maioli, A. Crut, F. Vallée and N. Del Fatti, *Adv. Opt. Mater.,* 2016, **4**, 567.

## 2 – Supplementary materials

**Table S1. Morphological features of the silica/polystyrene multipods used in this study and main side-products present in their batch**

| Targeted multipods | | Dodeca pods | Hexa pods | Tetra pods | Tri pods | Bi pods | Magnetic multipods [a] |
|---|---|---|---|---|---|---|---|
| Initial diameter of silica core (nm) [b] | | 85 | 85 | 85 | 45 | 40 | 100 ± 20 |
| Polystyrene satellite diameter (nm) [c] | | 85 | 140 | 160 | 155 | 180 | 140 |
| Final diameter of silica core (nm) | | 125 | 110 | 105 | 105 | 100 | 210 ± 20 |
| Morphology purity and main side-products (% with regard to the silica seeds) [d] | Monopods | - | - | - | 13 | 16 | - |
| | Bipods | - | - | - | 21 | **68** | 12 |
| | Tripods | - | 1 | 18 | **66** | 16 | 9 |
| | Tetrapods | - | 1 | **70** | - | - | 2 |
| | Pentapods | - | 5 | - | - | - | 5 |
| | Hexapods | - | **91** | 7 | - | - | 9 |
| | Heptapods | - | - | - | - | - | 1 |
| | Octopods | 3 | - | - | - | - | 10 |
| | Nonapods | 6 | - | - | - | - | 1 |
| | Decapods | 6 | - | - | - | - | 51 |
| | Hendecapods | - | - | - | - | - | |
| | Dodecapods | **75** | - | - | - | - | |
| | Multisilica [e] | 10 | 2 | 5 | - | - | - |

[a] after magnetic separation

[b] as measured from TEM images with polydispersity index lower than 1.01, excepted for the data of the last column

[c] as measured from TEM images on the targeted multipods

[d] as determined from TEM images and based on at least 500 observed objects, excepted for the data of the last column (about 150 observed objects)

[e] these are multipods containing two, rarely three, silica cores

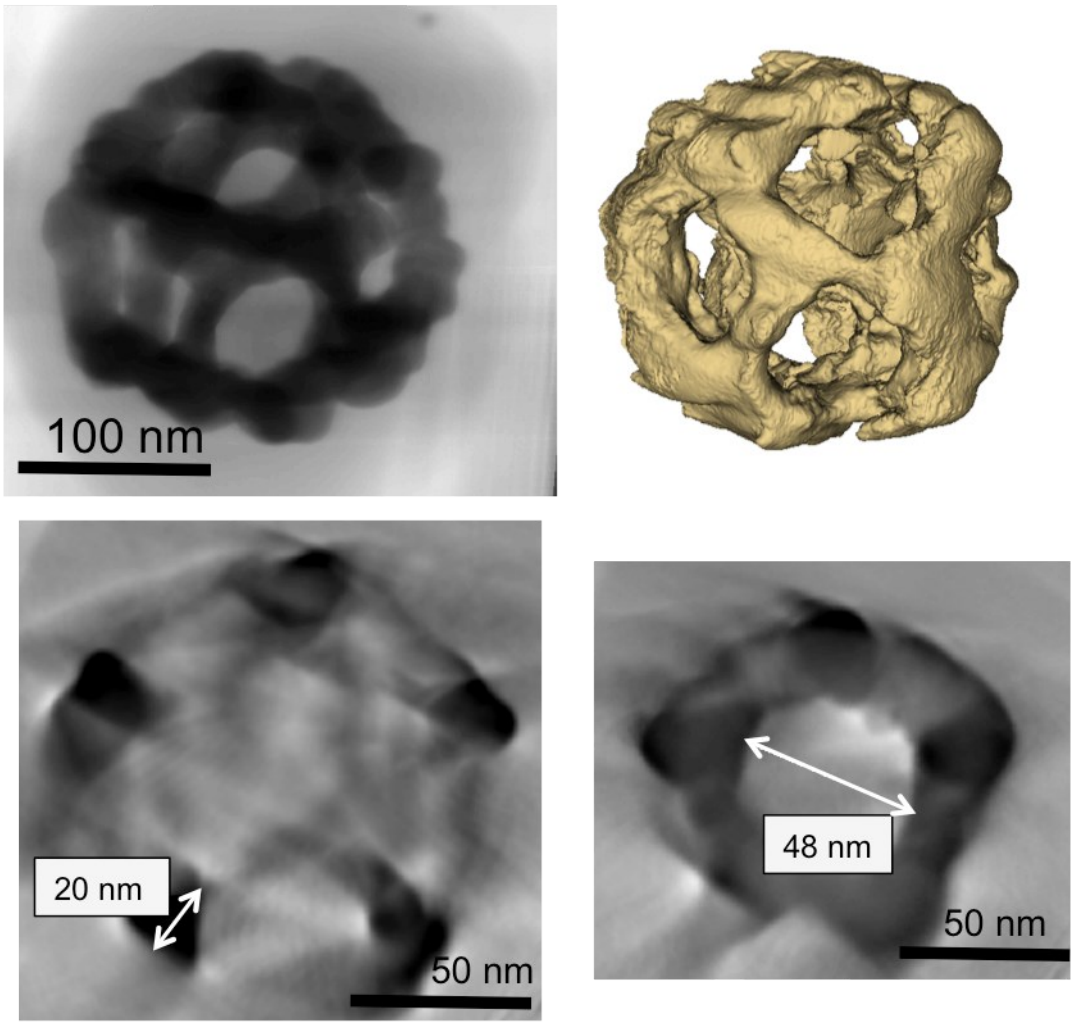


**Figure S1. TEM images from the tomography analysis of the nanocages with 12 windows and visualized 3D reconstruction. Slices through the different reconstructions are also displayed.**

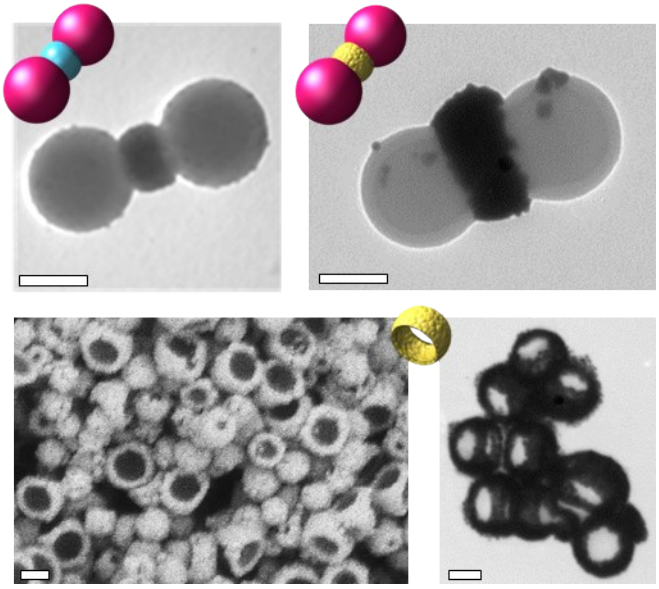

**Figure S2. TEM and SEM images of the different intermediates and resulting nanocages with two windows. Scale bars: 100 nm.**

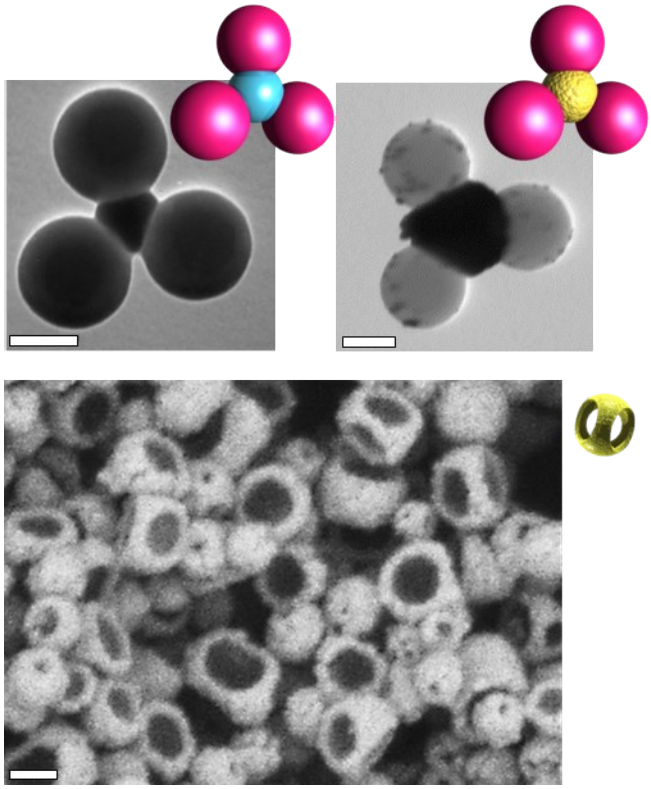

**Figure S3. TEM and SEM images of the different intermediates and resulting nanocages with three windows. Scale bars: 100 nm.**

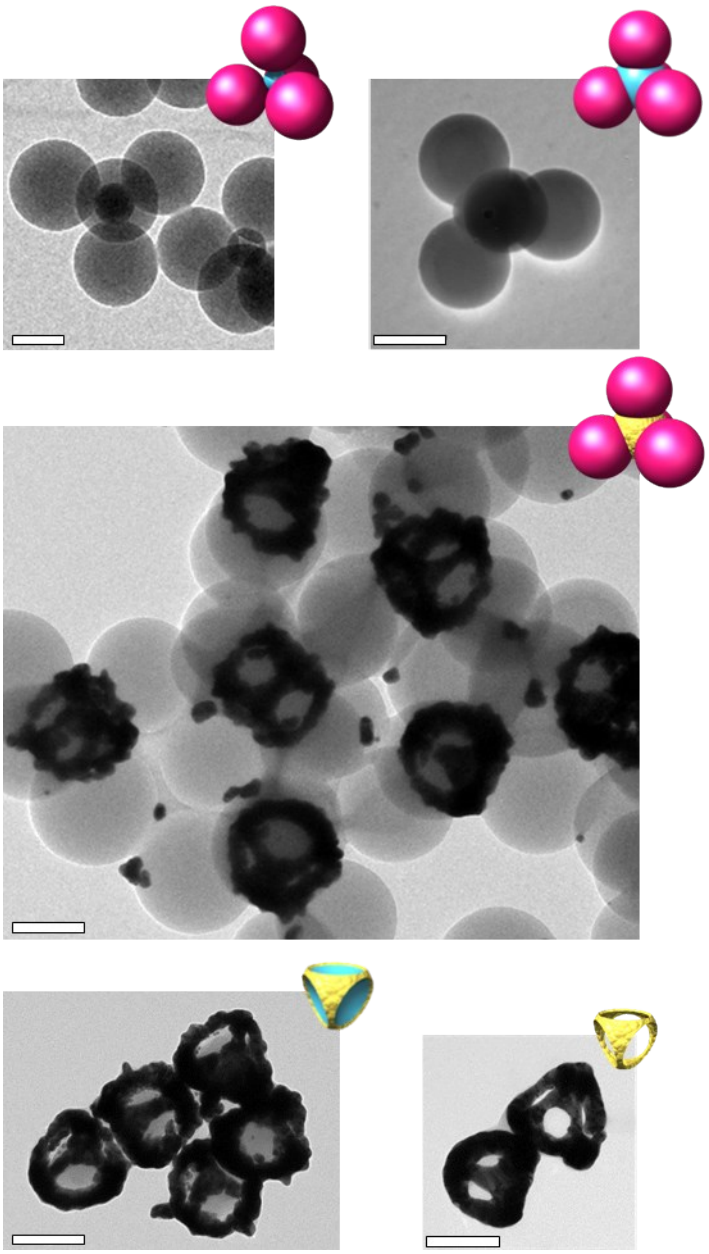

**Figure S4. TEM images of the different intermediates and resulting nanocages with four windows. Scale bars: 100 nm.**

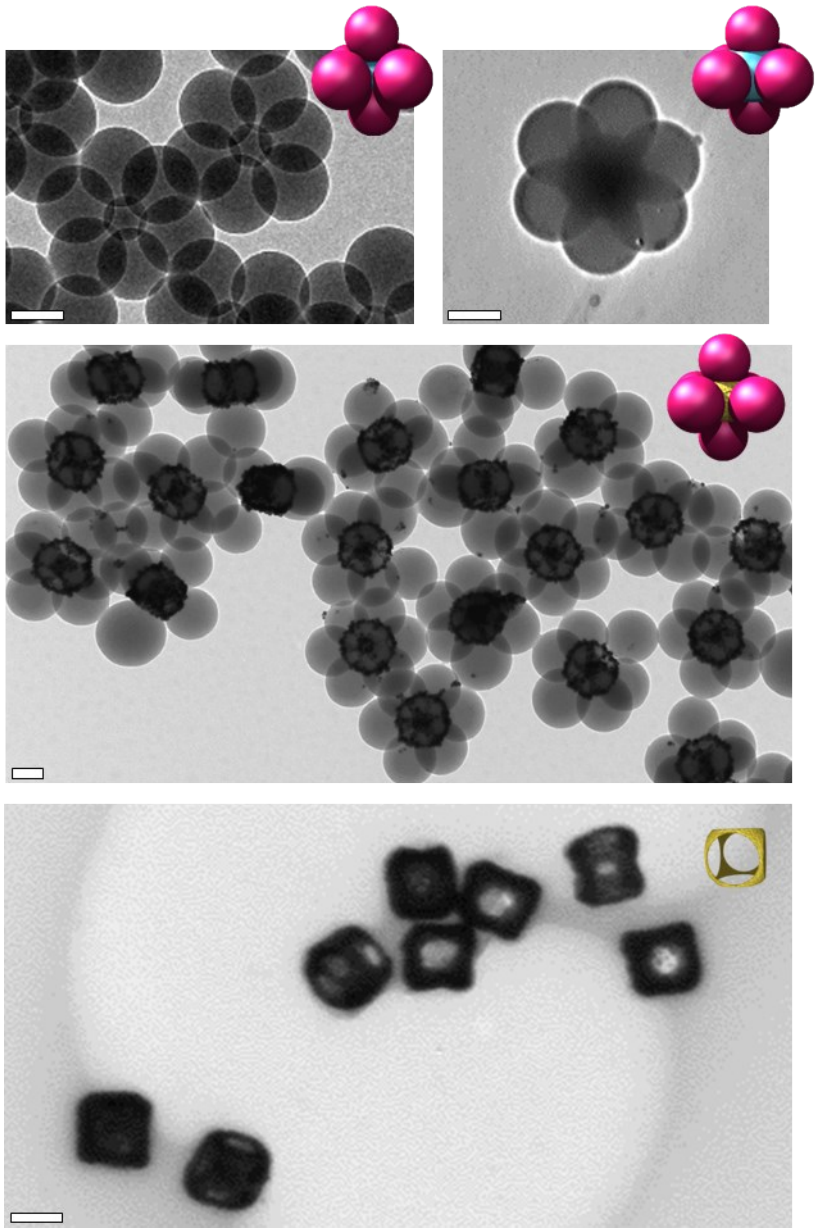

**Figure S5. TEM images of the different intermediates and resulting nanocages with six windows. Scale bars: 100 nm.**

**Table S2. Morphological features of the gold nanocages**

| Multipods-like templates | Dodeca pods | Hexa pods | Tetra pods | Tri pods | Bi pods |
|---|---|---|---|---|---|
| Window number | 12 | 6 | 4 | 3 | 2 |
| Internal diameter (nm) | 125 | 110 | 105 | 105 | 100 |
| Window diameter (nm) | 48 | 81 | 86 | 98 | 130 |
| Wall thickness (nm) | 20 | 22 | 32 | 28 | 30 |

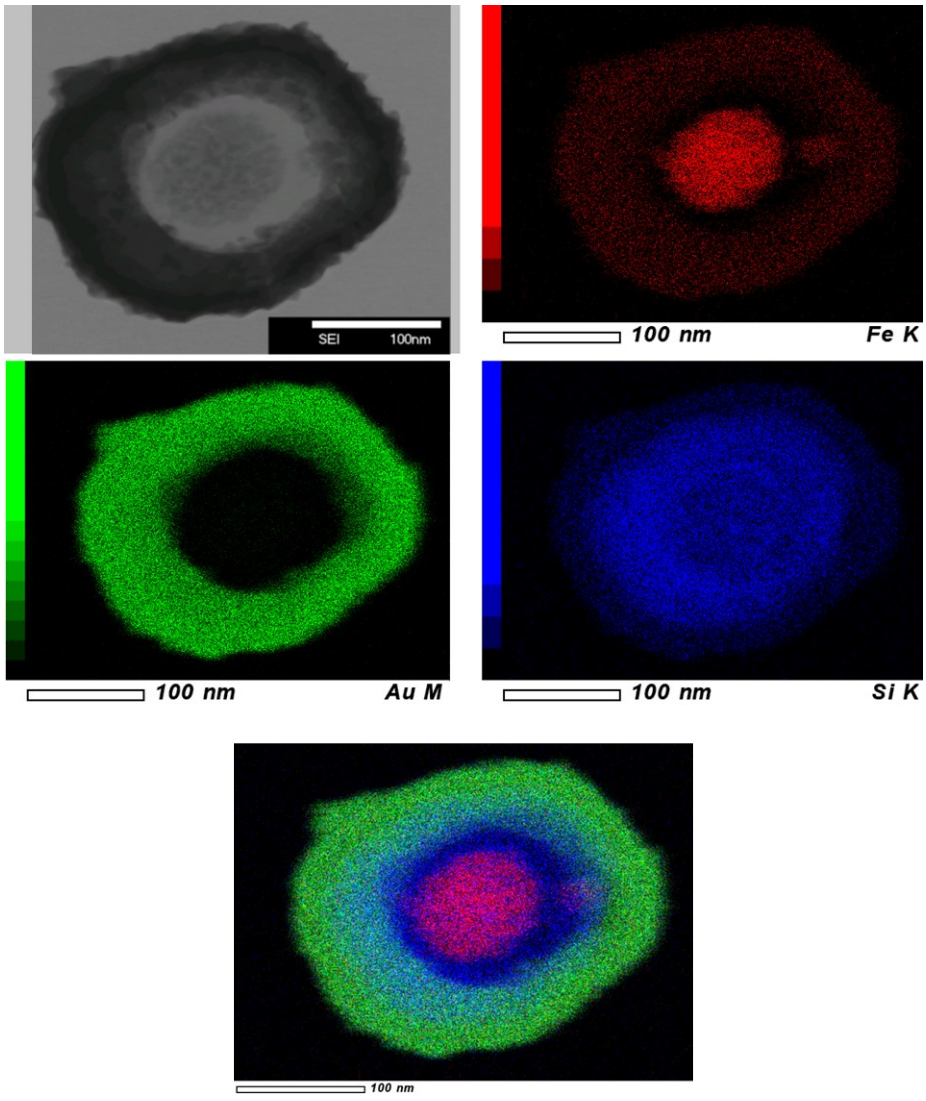


**Figure S6. STEM-EDX image and element mapping of a nanocage with two windows filled with a maghemite nanoparticle. Scale bars: 100 nm.**

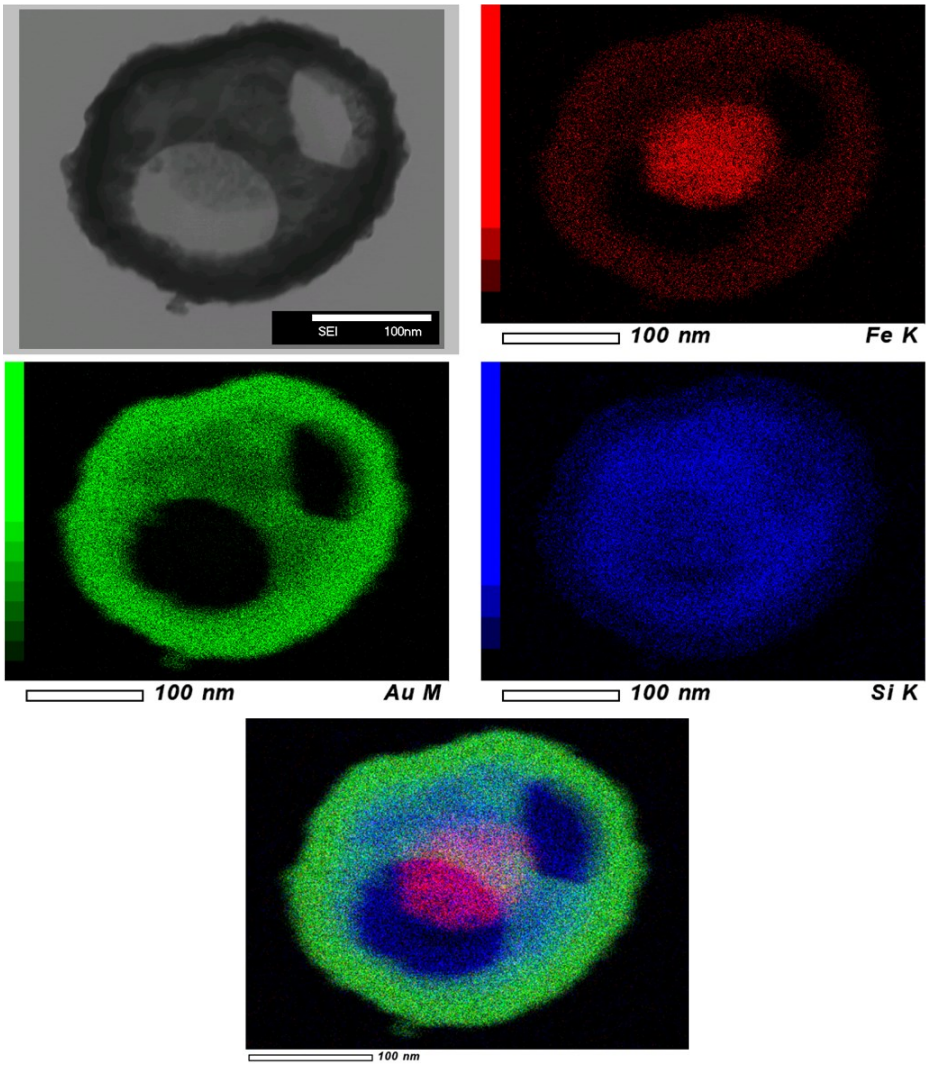


**Figure S7. STEM-EDX image and element mapping of a nanocage with three windows filled with a maghemite nanoparticle. Scale bars: 100 nm.**

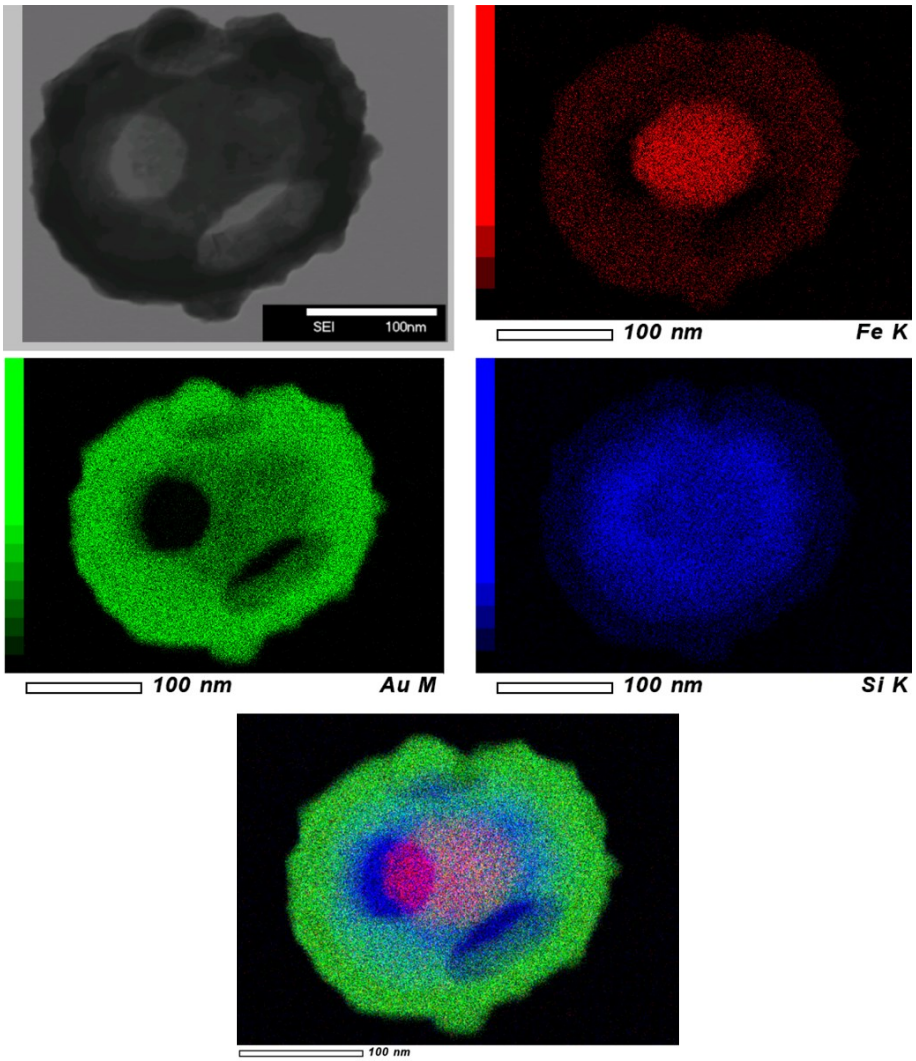


**Figure S8. STEM-EDX image and element mapping of a nanocage with four windows filled with a maghemite nanoparticle. Scale bars: 100 nm.**

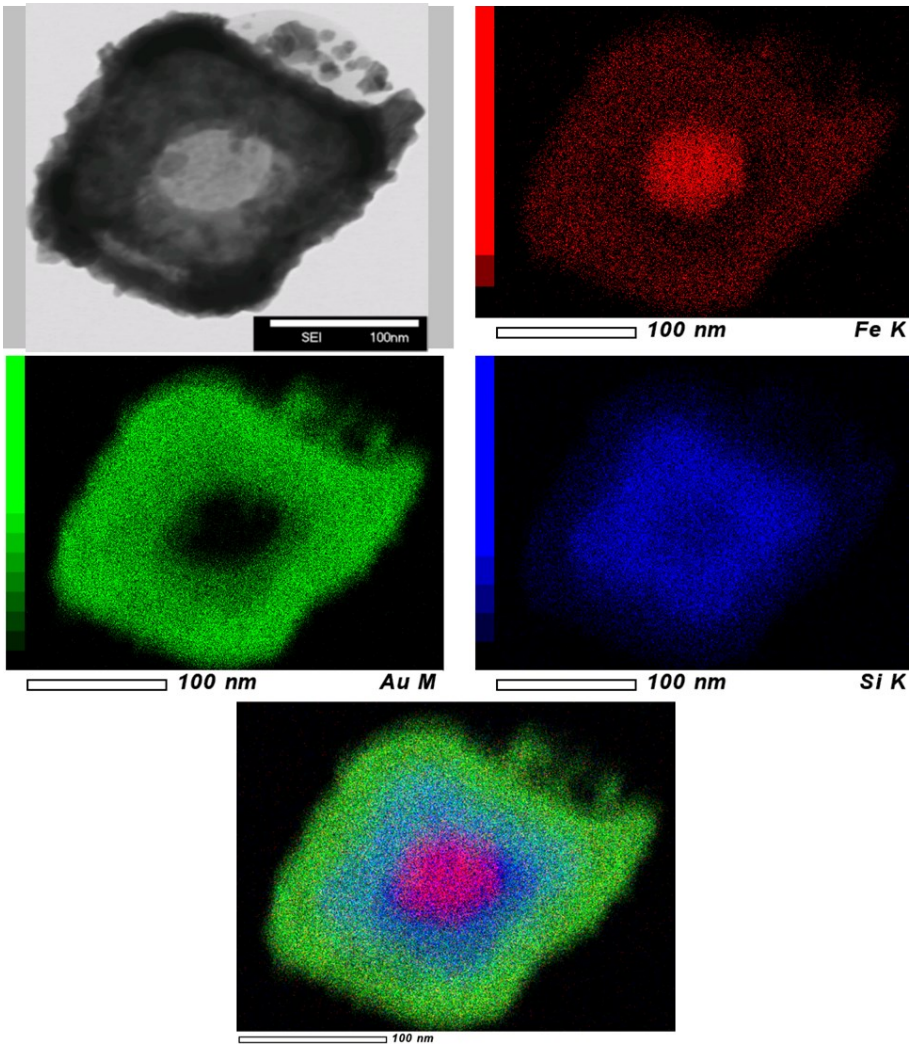


**Figure S9. STEM-EDX image and element mapping of a nanocage with six windows filled with a maghemite nanoparticle. Scale bars: 100 nm.**

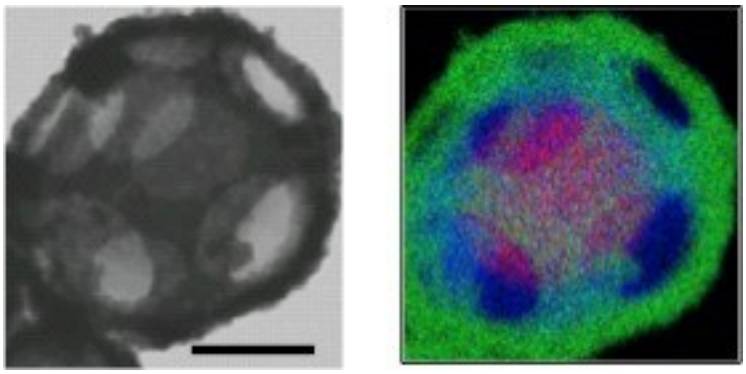

**Figure S10. STEM-EDX image and element mapping of a nanocage with twelve windows filled with a maghemite nanoparticle. The two images are at the same scale. Scale bar: 100 nm.**